The Effect of Strong Coulomb Correlations on Electron-Phonon Interactions in the Copper Oxides: Implications for Transport

Ju H. Kim[*], *K. Levin*[**], *R. Wentzcovitch*[†], *and A. Auerbach*[††]

[*] Department of Physics & Astronomy, The Johns Hopkins University, Baltimore, MD 21218
[**] The James Franck Institute, The University of Chicago, Chicago, IL 60637
[†] Department of Physics, Brookhaven National Laboratory, Upton, NY 11973
[††] Physics Department, Boston University, Boston, MA 02215

ABSTRACT

The effects of strong Coulomb correlations on the electron-phonon interactions in the high temperature superconductors are investigated. Very strong Coulomb correlations, which are essential for creating the insulating state at half filling, lead to a suppression of charge fluctuations as the insulator is approached. This thereby significantly reduces the electron-phonon coupling. We present a self-consistent "frozen phonon" scheme which is based on a Coulomb renormalized band structure of the copper-oxygen plane as a method for calculating these effects and their influence on transport properties. The microscopic spectral function has a two-peak structure, each peak of which can be associated with primarily copper-like and oxygen-like motion. A high density of these low frequency copper-dominated modes is important, for it leads to a linear resistivity extending down to temperatures of the order of 50K. A Drude fit to low frequency ac conductivity measurements yields a decrease in the plasma frequency as the insulator is approached, as well as a relatively concentration x independent scattering time τ. The magnitude of the latter provides an upper bound on the electron-phonon coupling constant, which is found to be rather weak (λ<0.2-0.4) in accord with our calculations. The behavior of the calculated plasma frequency is also consistent with experiment and its x dependence is associated with an increase in the effective mass, due to incipient localization, as the insulator is approached. On the other hand, the calculated x independence of the electron-phonon contribution to the resistivity is not compatible with the increase observed in the **total** resistivity slope as the insulator is approached. This suggests that the phonon background accounts for a significant fraction of the measured resistivity slope at high x, but this contribution is not sufficient to explain the behavior at smaller x. Thus electron-electron or magnetic scattering may be playing a more dominant role near the insulator. Following the Mott-Ioffe-Regel criterion, we find that this additional scattering is crucial for the break-down of the metallic state at finite doping concentrations.

1. Introduction

The normal and superconducting states of the copper oxides have been vigorously investigated since the discovery of high temperature superconductivity. Because of the complex phase diagram[1] of these materials (Fig. 1), there is yet no clear consensus on the correct description of the normal state. It has been suggested[2] that the temperature and frequency dependence of transport and magnetic measurements are incompatible with Fermi liquid theory. In this paper we consider this question further with emphasis on electron-phonon coupling and its implications for transport. In order to gain insight into the copper oxides, we have made an extensive phenomenological

This work was supported by US DOE under contract no. DE-AC02-76CH00016.

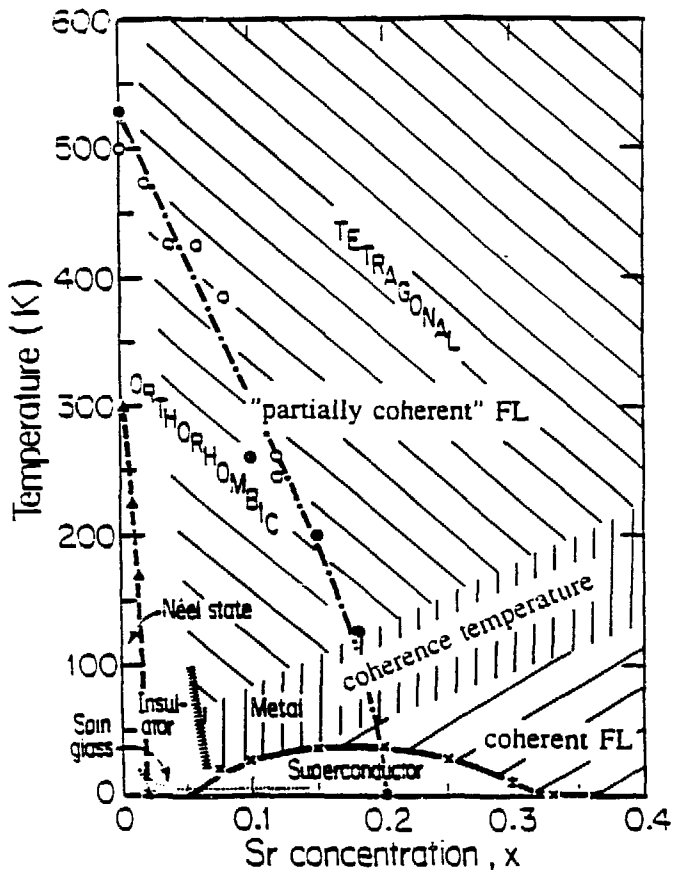

Fig. 1 The proposed phase diagram for a Fermi liquid.

comparison[3] with another class of strongly correlated metals, the heavy fermions. We find remakable similarities between these two systems. Unlike the copper oxides, the normal state of the heavy fermions is reasonably well characterized and appears to correspond to a canonical Fermi liquid[4] at temperatures low compared to the coherence temperature T_{coh}. Above T_{coh} the breakdown of the quasiparticle state occurs and the f electrons become progressively more localized and therefore incoherent. The temperature and frequency dependent normal state properties above this energy show a considerable departure from usual Fermi liquid behavior, much as is seen in the cuprates above T_c. Based on this phenomenological evidence and on microscopic calculations of transport[5] and magnetic properties of the copper oxides[6], we propose a phase diagram[7] for the cuprates which is similar to that of the heavy fermions. This is presented in Fig. 1 with $La_{2-x}Sr_xCuO_4$ as an example. In this phase diagram the key parameter is T_c/T_{coh}. Only when this is sufficiently small, can one see classical Fermi liquid properties of the normal state. [Here the coherence temperature is shown as a slightly extended region, since T_{coh} appears to vary slightly, depending on the experimental probe]. Since T_{coh} decreases as $x \rightarrow 0$, one expects marginal (or partially coherent) Fermi liquid-like behavior above T_c at low x. By contrast in the over-doped regime canonical Fermi liquid behavior should be evident above T_c.

In summary, we propose that the unusual temperature and frequency dependent behavior in the copper oxides arises as a consequence of the gradual evolution of the Fermi liquid ground state into a partially coherent state as either x is decreased or temperature is increased. In what follows we will discuss how normal state transport such as the electrical resistivity and ac conductivity provide support for the proposed Fermi liquid phase diagram shown in Fig. 1.

2. Summary of Transport Behavior

The temperature-dependent resistivity ρ of an optimally doped sample (x=0.15 in $La_{2-x}Sr_xCuO_4$) is strictly linear and often extrapolates to a zero intercept value.[8] How universal is this temperature dependence when the doping concentration is varied? In Fig. 2 the concentration dependent resistivity for both a La[9] and a Tl-based compound[10] is shown. The letters A to D in Fig. 2(b) correspond to increasing x, i.e. overdoping, which is associated with the addition of oxygen. In the Tl (2201) system, for temperatures above roughly 200K, the resistivity is linear for all x. The resistivity, below 200K, however, depends strongly on x. As shown in the figure the low temperature resistivity of an overdoped sample exhibits more Fermi liquid-like T^2 behavior. As x is decreased to approach optimal doping, however, the T^2 behavior disappears and ρ becomes linear. In the 214 system as x is further decreased towards 0, the linear resistivity again disappears and the behavior is consistent with a semiconducting or insulating state.

The resistivity slope dρ/dT at 300K shown in Fig. 2(a). This slope increases rapidly as the metal-insulator transition is approached. By contrast, for the overdoped samples shown in Fig. 2(b), the slope is almost concentration independent.

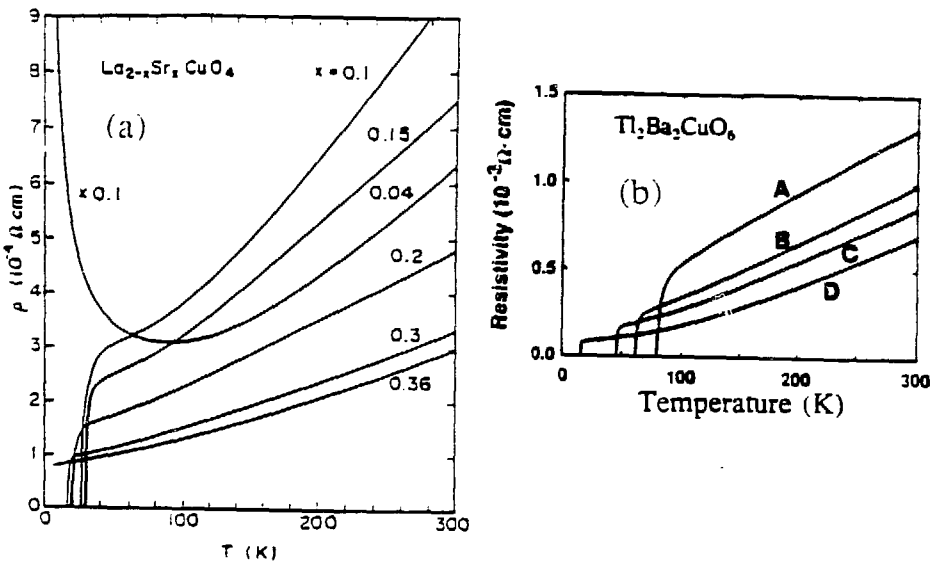

Fig. 2 The temperature dependent resistivity for both a (a) La (214) and a (b) Tl (2201) based compound.

Because of this ubiquitous linear behavior, the temperature dependent resistivity in the metallic oxides has received considerable attention. One may ask, then, how unique is this behavior? This may, best, be answered by comparison with other strongly correlated systems, such as the heavy fermion metals. For some heavy fermions, a Fermi liquid (T^2) signature is never observed in the normal state (at ambient pressures). This is illustrated by studies[11] of UBe_{13} in Fig. 3. Here at ambient pressure, it appears that T_c/T_{coh} is sufficiently large to block "access" to the canonical Fermi liquid state. Only when strong pressure is applied (thereby reducing T_c/T_{coh}) is the conventional T^2 dependence observed. At all pressures there appears to be a linear regime for some range of temperatures (above the T^2 regime) followed by a tendency towards saturation. It is generally believed that a linear dependence in ρ will occur at temperatures high compared to the characteristic energy scale of the bosons[12] which mediate interactions between quasiparticles. These bosons may correspond to phonons (which are external to the electronic system) as well as to electronic excitations. In the heavy fermion problem the energy scale corresponds to T_{coh} for the electronic case. For phonons, quite generally the energy is (some fraction of) the Debye energy ω_D. It is important to stress that in the heavy fermion system, while a linear resistivity appears to also be ubiquitous, at sufficiently high T, it appears for only a limited temperature range. This is clearly in contrast with the cuprates, where the linear regime is quite extensive.

Further comparison between the heavy fermion systems and the cuprates is shown in Fig. 4. Here a similarity between $YBa_2Cu_3O_{7-\delta}$ and UPt_3 is observed in ac conductivity measurements.[13] We have rescaled the horizontal axis in a consistent fashion, in Fig. 4(b) to represent the phenomenological observation that the appropriate T_{coh} for

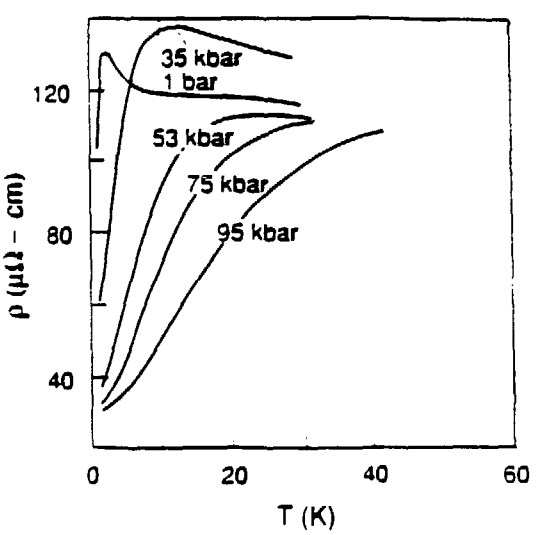

Fig. 3 The pressure dependent resistivity of UBe_{13}.

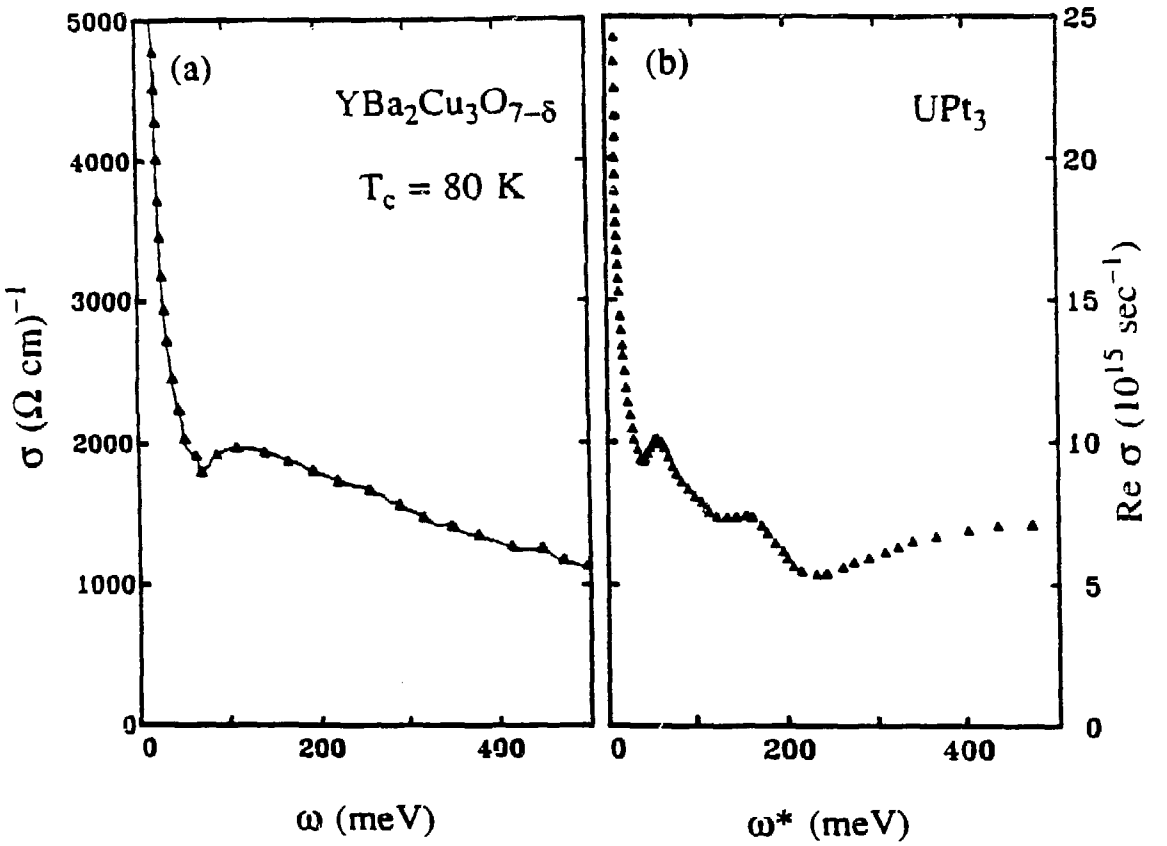

Fig. 4 The frequency dependence of ac conductivity for (a) $YBa_2Cu_3O_{7-\delta}$ (T_c=80K) and (b) UPt_3.

UPt_3 is smaller than for $YBa_2Cu_3O_{7-\delta}$. The two plots show a Drude-like conductivity at low frequency with structure in the spectrum at higher frequencies. Although the origin of a midinfrared peak in the copper oxides is, still, controversial, this structure, in UPt_3 at 5K, is related to coherence effects since measurements at room temperature shows no such peaks.[14]

Drude ac conductivity allows one to separate the scattering lifetime τ and the plasma frequency ω_p. This measured dc lifetime, therefore, sets a limit on the strength of coupling of the electrons to any scattering mechanism (boson). In the cuprates this analysis suggests that the coupling constant[15] is λ~0.2–0.4. The same analysis shows that the concentration dependent plasma frequency ω_p is found to vary $\omega_p^2 \propto x$. This behavior may be interpreted as either suggesting a doped semiconductor picture ($n \propto x$) or a heavy Fermi liquid ($m^* \propto 1/x$). In Fig. 5, the effective mass m^* of an electron in units of the band mass for $YBa_2Cu_3O_{7-\delta}$ is plotted as a function of T_c.[16] Decreasing T_c is equivalent to decreasing x. A rapid increase of the effective mass near the insulator is obtained from the Fermi liquid interpretation. This suggests incipient localization[17] as the insulator is approached.

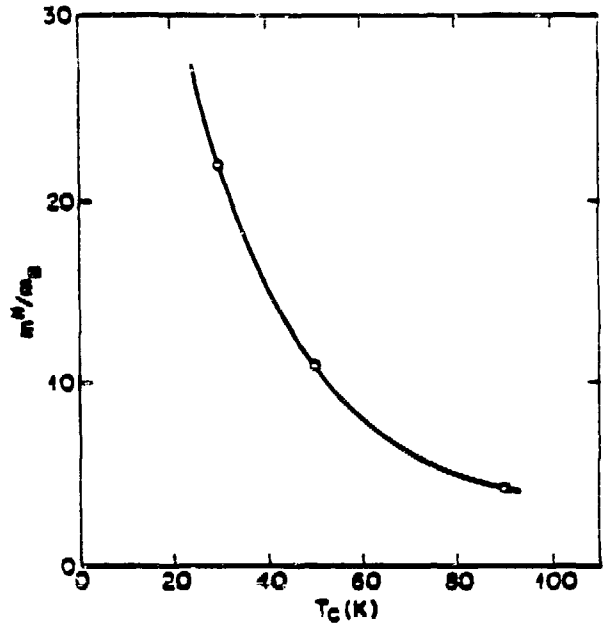

Fig. 5 The effective mass of an electron for $YBa_2Cu_3O_{7-\delta}$ as a function of T_c.

Based on the evidence discussed above, as well as on phenomenological comparisons made elsewhere,[3] the heavy Fermi liquid analogy for the copper oxides is a useful starting point. In addition to these phenomenological similarities, the underlying Hamiltonians of the two systems are similar: both consist of (essentially) two hybridized bands, with strong Coulomb correlations on one component (d for the cuprates) and (f for the heavy fermions). Within this framework the remainder of this paper addresses the following three questions (1) If copper d-electrons are "quasi-localized" because of strong Coulomb correlations then how will this affect electron-phonon interactions. (2) To what extent does the electron-phonon background contribute to the resistivity. (3) And what is the nature of the breakdown of Fermi liquid as the insulator is approached.

3. Renormalized Band Structure for the Copper Oxides

Our construction of a Fermi liquid picture for the copper oxides includes two main ingredients. (1) We adopt reasonable values for the copper-oxygen hybridization V and the oxygen-oxygen hopping t in the infinite U_d extended Hubbard Hamiltonian.[7] This allows us to obtain a semi-realistic renormalized band structure which will be the basis for our transport calculations. (2) We assume a breakdown of the Fermi liquid state occurs by Brinkman-Rice localization.[18] Here the antibonding band narrows as half filling is approached due to strong Coulomb correlations. This is consistent with increasing effective mass as the insulator is approached, as found in the plasma frequency measurements discussed above.

Our starting point is the 3-band Hubbard Hamiltonian which describes the copper oxide plane. We include a next-nearest neighbor interaction (i.e., oxygen-oxygen overlap)

$$H = \sum_{j,\sigma}\varepsilon_p C^{\dagger}_{j,\sigma}C_{j,\sigma}+\sum_{i,\sigma}\varepsilon_d^{o} D^{\dagger}_{i,\sigma}D_{i,\sigma}+ \sum_{<ij>,\sigma} V(C^{\dagger}_{j,\sigma}D_{i,\sigma}+ h.c.) + \sum_{<jl>,\sigma} t(C^{\dagger}_{j,\sigma}C_{l,\sigma}+ h.c.) + \sum_{i} U_d n_{i,\uparrow}n_{i,\downarrow} \quad (1)$$

where ε_p and ε_d^{o} are the oxygen and (unrenormalized) copper energy levels, $C^{\dagger}_{j,\sigma}$ ($C_{.,\sigma}$) and $D^{\dagger}_{i,\sigma}$ ($D_{i,\sigma}$) are creation (destruction) operators for the oxygen electrons at site j and spin σ and copper electrons at site i, with spin σ respectively. The hopping interaction V is between neighboring copper and oxygen sites, while t is the transfer integral between two nearest neighboring oxygen sites, and $n_{i,\sigma}=D^{\dagger}_{i,\sigma}D_{i,\sigma}$. The Coulomb repulsion between electrons on a Cu site is U_d.

The above Hamiltonian is simplified by employing a well known auxiliary bosonization technique[19] to characterize the three valence states of Cu. In the infinite Coulomb correlation limit we write the copper electron operator $D^{\dagger}_{i,\sigma}$ in Eq. 1 in terms of boson and fermion state operators as

$$D^{\dagger}_{i,\sigma} = d^{\dagger}_{i,\sigma}e_i \, . \quad (2)$$

Here, the operators $d^{\dagger}_{i,\sigma}$ and e_i represent the creation operator for a singly occupied state (Cu^{2+}) and the destruction operator for an empty (Cu^{3+}) state. The doubly occupied state (Cu^{1+}) has been projected out due to $U_d=\infty$. (It should be noted that an alternative "hole picture" description can also be shown to lead to similar results, provided the parameters are chosen so that Mott or Brinkman-Rice localization occurs at half filling.) Within this approach the Hamiltonian in Eq. 1 is rewritten as

$$H_o = \sum_{j,\sigma}\varepsilon_p C^{\dagger}_{j,\sigma}C_{j,\sigma}+\sum_{i,\sigma}\varepsilon_d^{o} d^{\dagger}_{i,\sigma}d_{i,\sigma}+ \sum_{<ij>,\sigma} V(C^{\dagger}_{j,\sigma}e_i^{\dagger}d_{i,\sigma}+ h.c.)+ \sum_{<jl>,\sigma} t(C^{\dagger}_{j,\sigma}C_{l,\sigma}+ h.c.) \, . \quad (3)$$

Furthermore a completeness relation

$$\sum_{\sigma} d^{\dagger}_{i,\sigma}d_{i,\sigma} + e_i^{\dagger}e_i = 1 \quad (4)$$

must be imposed to ensure that all copper states are accounted for.

In mean field theory,[17] a renormalized band structure is obtained by adding Eq. 4 with a Lagrange multiplier λ_i to Eq. 3 and, then, by variationally minimizing the free energy with respect to the parameters $e_o=\langle e_i\rangle$ and $\lambda_o=\langle\lambda_i\rangle$. Infinite Coulomb correlations at the mean field lead to two effects: first, the hybridization is renormalized as follows

$$V \rightarrow e_o V \quad (5a)$$

and the copper d-level is shifted as

$$\varepsilon_d^{o} \rightarrow \varepsilon_d^{o}+\lambda_o \quad (5b)$$

These two renormalizations are necessary to avoid multiple occupancy of the copper

level. The hybridization reduction factor is given by the bose amplitude e_b where $e_b^2=1-n_d$ and $n_d \leq 1$ is the number of copper electrons at each site. As the system approaches the insulating state $e_b \rightarrow 0$ and $n_d \rightarrow 1$, and at the same time the effective mass $m^* \rightarrow \infty$.

4. Frozen Phonon Scheme

Our semi-realistic model allows us to consider various phonons in the copper-oxygen plane. We calculate self-consistently the electron-phonon interaction[5] by considering the change in electronic structure resulting from a static lattice distortion. To carry out an explicit calculation, we consider only the case of doubling of the unit cell which corresponds to a zone edge phonon (**q**=**X**). This frozen phonon method is often used to deduce electron-phonon coupling in the context of more conventional band structure approaches. Here we extend this formalism to include strong Coulomb correlations and apply it to the copper oxide plane. Our work builds on an earlier lattice dynamics calculation[20] which has identified normal mode displacements and frequencies. By way of simplification we categorize seventeen stable modes into six distinct types (as shown in Fig. 6) of motion of the ion *within* the copper-oxygen plane.

The Hamiltonian for the distorted (**X**-mode) lattice is written as

$$H_{FP}^{2d} = \sum_{i,\mu,\sigma} \varepsilon_{d,\mu}^{o} d_{i,\mu,\sigma}^{\dagger} d_{i,\mu,\sigma} + \sum_{i,nu,\eta,\sigma} \varepsilon_{p,\nu}^{\eta} C_{i,\nu,\sigma}^{\eta\,\dagger} C_{i,\nu,\sigma}^{\eta} + \sum_{i,\mu,\sigma} V_{\mu} (d_{i,\mu,\sigma}^{\dagger} e_{i,\mu} \sum_{\delta,\nu,\eta} C_{i+\delta,\nu,\sigma}^{\eta} + \text{h.c.})$$
$$+ \frac{1}{2} \sum_{i,\nu,\nu',\sigma} (C_{i,\nu,\sigma}^{\eta\,\dagger} \sum_{\delta,\eta' \neq \eta} t_{\delta} C_{i+\delta,\nu',\sigma}^{\eta'} + \text{h.c.}) \qquad (6)$$

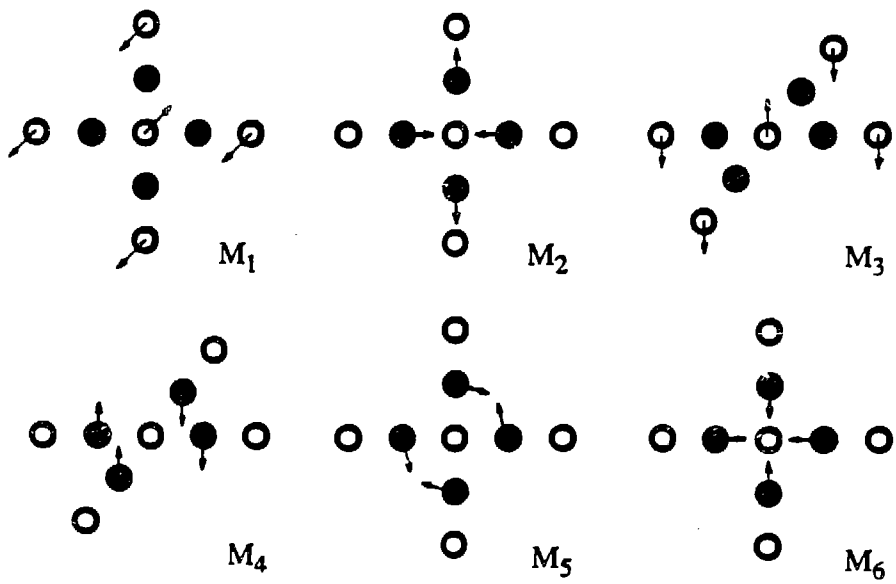

Fig. 6 The six planar modes projected from the lattice dynamics calculation of Ref. 20. The open and closed circles indicate copper and oxygen, respectively.

where the index μ=1,2 denotes two positions for the copper orbitals and the indices ν(=1,2) and η(=x,y) denote two oxygen sites with orbitals (p_x,p_y). V_μ and t_δ denote changes in the Hamiltonian parameters resulting from the displacement of ions about their equilibrium position. Following the work[2] of Slater and Koster we can evaluate these changes microscopically. The overlap integral between copper and oxygen orbitals depends strongly on the separation distance and is highly anisotropic. A small distortion along the longitudinal (bonding axis) leads to significant changes in hybridization. These can be represented as linearly proportional to the ionic displacement when the distortion is small

$$V(\mathbf{R}+\delta\mathbf{R})-V(\mathbf{R}) = \frac{\delta V}{\delta \mathbf{R}}\cdot\delta\mathbf{R} = -7V(\mathbf{R})\frac{\delta R}{a} \tag{7a}$$

and

$$t(\mathbf{R}+\delta\mathbf{R})-t(\mathbf{R}) = \frac{\delta t}{\delta \mathbf{R}}\cdot\delta\mathbf{R} = -2t(\mathbf{R})\frac{\delta R}{a} \ . \tag{7b}$$

These changes in V and t ultimately lead to changes in the variational parameters such as e_μ and λ_μ. When these parameters are self-consistently calculated they are found to vary linearly with displacement about the equilibrium (or undistorted) values e_o and λ_o

$$e_\mu = e_o \pm \frac{\delta e_o}{\delta \mathbf{R}}\cdot\delta\mathbf{R} \tag{8a}$$

and

$$\lambda_\mu - \lambda_{\mu'} = \frac{\delta\lambda_o}{\delta \mathbf{R}}\cdot\delta\mathbf{R} \tag{8b}$$

where $\delta e_o/\delta R$ and $\delta\lambda_o/\delta R$ may be identified as the Coulomb correlation induced screening responses. These functions depend on E_F.[5,7]

The electron-phonon interaction term is calculated by taking the difference between the Hamiltonians corresponding to the distorted and undistorted configurations and writing

$$H_{el-ph} = H_{FP}^{2d} - H_o = \sum_{k,\sigma,\nu} g_{X,\nu}\left[\frac{1}{2N_oM_{X,\nu}\omega_{X,\nu}}\right]^{\frac{1}{2}} \alpha^{+}_{k,\sigma}\alpha_{k+X,\sigma}(a^{+}_{X,\nu} + a_{-X,\nu}) \tag{9}$$

where $\alpha^{+}_{X,\sigma}$ is a creation operator for a quasiparticle in the antibonding band which is derived from mixing $3d_{x^2-y^2}$, $2p_x$, and $2p_y$ orbitals. N_o is the number of ions in each unit cell and $M_{X,\nu}$ is the reduced mass corresponding to a phonon mode ($\mathbf{X}$,ν). Here $\omega_{X,\nu}$ is a normal mode frequency. The transition matrix element $g_{X,\nu}$ is written as

$$g_{X,\nu} = \lim_{\delta R\to 0} \langle\alpha_{k,\sigma}|\frac{\delta H}{\delta \mathbf{R}}\cdot\hat{\epsilon}_{X,\nu}|\alpha_{k+X,\sigma}\rangle \tag{10}$$

where $\hat{\epsilon}_{X,\nu}$ is the polarization vector. Here we focus on intraband scattering, in the antibonding band, between states $\mathbf{k}$ and $\mathbf{k+X}$ because these states near E_F are strongly scattered by the ionic displacement. The interband scattering processes require higher energies than can be provided by a phonon.

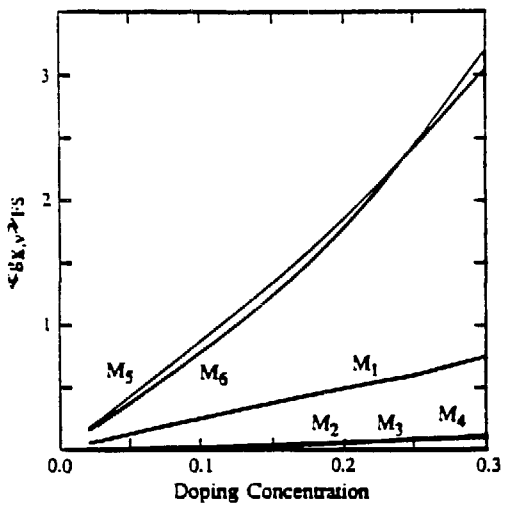

Fig. 7 Concentration dependence of the Fermi surface averaged electron-phonon transition matrix elements for the six modes shown in Fig. 6.

In Fig. 7, we plot the Fermi surface average $\ll \gg_{FS}$ of the resulting electron-phonon matrix elements for the six types of X-phonons shown in Fig. 6 as a function of concentration. It is clear from Fig. 7 that charge transfer modes M_1, M_5, and M_6 couple to the electrons more strongly than others although they are still weak compared to the zero Coulomb correlation case. It is shown, elsewhere, analytically[5,7] that various $\ll g_{X,\nu} \gg_{FS}$ all vary as powers of e_0^2, which vanishes at the metal-insulator transition. However, near this transition the frozen phonon picture will break down[5] since there the electronic energy scales become comparable to those of the phonons due the narrowing of the antibonding band.

5. Transport Properties

In this section we discuss the implications of the frozen phonon calculations for transport properties. We also compare our results with experiment.

In Fig. 8 the electron-phonon transport spectral function

$$\alpha_{tr}^2 F(\omega) = \frac{\ll [v_{kx} - v_{k'x}]^2 g_{X,\nu}^2 \gg_{FS}}{4 \ll v_{kx}^2 \gg_{FS}} \frac{\hbar N(E_F)}{N_1 M_\nu \omega_{X,\nu}} \delta(\omega - \omega_{X,\nu}) \qquad (11)$$

is plotted for $t/V = 0.25$ and $x=0.15$. In this calculation the microscopically determined transition-matrix elements are used for the evaluation of α_{tr}^2. A rough fit of our microscopically derived $\alpha_{tr}^2 F(\omega)$ yields a double-peak structure with each peak associated with a predominantly Cu-like or O-like mode where low and high frequency peaks are from copper and oxygen motion, respectively. In the inset, we compare the phonon density of states $F(\omega)$ obtained from neutron data[22] on $La_{1.85}Sr_{0.15}CuO_4$ with that obtained from the lattice dynamics calculation (shaded histogram). As illustrated in the figure, the calculated $F(\omega)$ qualitatively reproduces the general features of the experimental results.

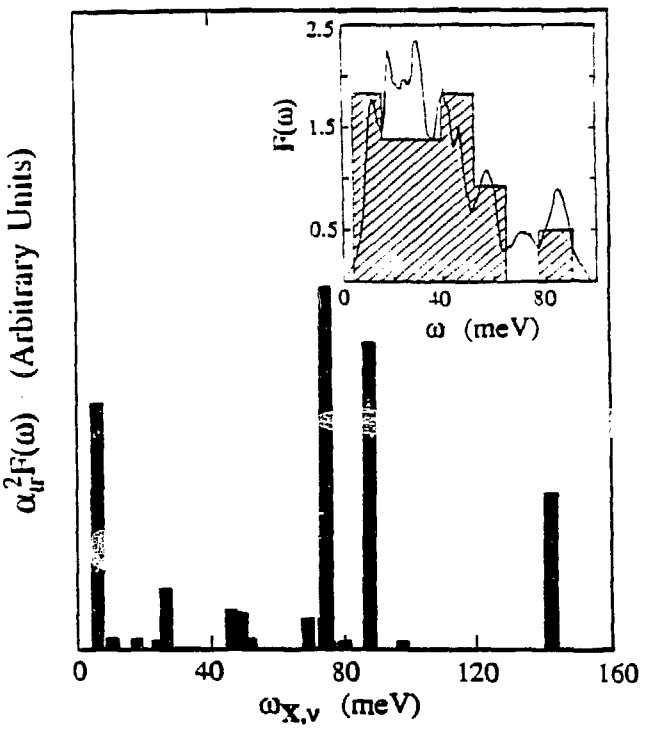

Fig. 8 Electron-phonon transport spectral function for t/V=0.25 and x=0.15. In the inset, the phonon density of states from Ref. 22 is plotted to compare with the results obtained from rescaling the lattice dynamics calculation (shaded region) of Ref. 20.

The electron phonon scattering rate is

$$\frac{1}{\tau_{el-ph}} = \frac{4\pi k_B T}{\hbar} \int d\omega\, \alpha_{tr}^2 F(\omega) \frac{I(\omega/2k_B T)}{\omega} \tag{12}$$

which is plotted in Fig. 9(a). Here

$$I(x) = \left(\frac{x}{\sinh x}\right)^2 . \tag{13}$$

The solid curve denotes the scattering lifetime arising from electron-phonon interactions. Due to the vanishing electron-phonon transition matrix element near the metal-insulator transition the lifetime increases rapidly as the insulator is approached. This large lifetime can, however, be cut off by the presense of either electron-electron or magnetic scattering. When a phenomenological lifetime of the form $1/\tau_o \propto N(E_F)T$ is added to the electron-phonon contribution the overall lifetime (shown by the dotted line) is consistent with the relatively concentration independent data plotted in Fig. 9(b).[23,24] This analysis suggests that mechanisms other than electron-phonon scattering must be invoked near the metal insulator transition. The semi-quantitative agreement between the electron-phonon induced lifetime and the data at large x shows that our electron-phonon coupling constant λ_{el-ph} defined by $\tau^{-1}=2\pi\lambda_{el-ph}T$ is consistent with the upper bound 0.2-0.4 which is determined experimentally.

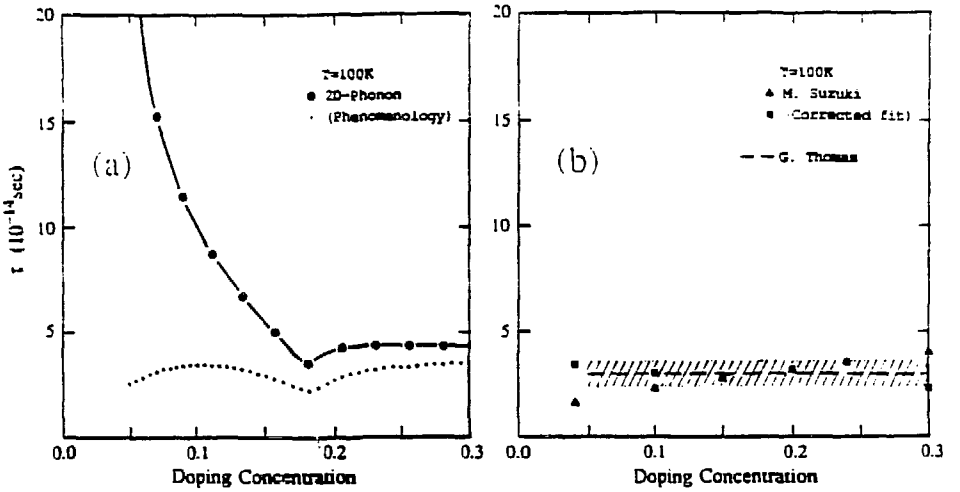

Fig. 9 (a) Concentration dependence of the transport lifetime at 100K and t/V=0.25 with (or without) a small phenomenologically added lifetime as shown by the dotted (or solid) line. (b) Experimentally measured transport lifetime. "Corrected fit" in Fig. 9(b) corresponds to fitted data (square) in Fig. 10(b).

The plasma frequency as a function of x plotted in Fig. 10(a) is calculated from

$$\omega_p^2 = 4\pi e^2 \sum_k v_{kx}^2 \delta(E_k - E_F) \ . \qquad (14)$$

As shown in the figure, ω_p varies roughly as $x^{1/2}$. Structure near x=0.15 is due to the van Hove singularity. It should be noted that this x dependence is consistent with

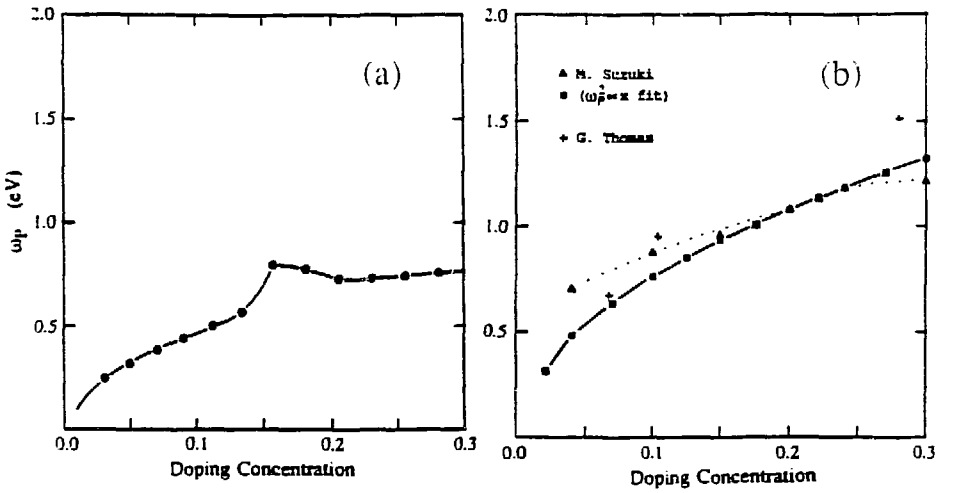

Fig. 10 (a) Concentration dependence of the plasma frequency for t/V=0.25. (b) Experimentally measured plasma frequency. The triangles in Fig. 10(b) indicate strontium doping in La_2CuO_4 from Ref. 24 and the squares represent a $\omega_p^2 \propto x$ fit of this data. The crosses indicate oxygen concentration dependence in $YBa_2Cu_3O_{7-\delta}$ from Ref. 23 scaled to an effective hole concentration x.

optical data[23,24] summarized in Fig. 10(b) for both $La_{2-x}Sr_xCuO_4$ and $YBa_2Cu_3O_{7-\delta}$.

By way of summary we show the data for the resistivity slope dρ/dT as a function of x on $La_{2-x}Sr_xCuO_4$ at 300K taken by several groups in different symbols (squares,[25] triangles,[9] crosses,[26] and circles[27]) in Fig. 11. In the inset, we plot the temperature-dependent resistivity ρ as calculated from

$$\rho_{el-ph}(T) = 4\pi\frac{\Omega_o}{\omega_p^2}\frac{1}{\tau_{el-ph}(T)} . \qquad (15)$$

Although the inset curve is quasi-linear down to low temperatures it is not precisely linear. This nearly linear resistivity at low temperature is derived from low frequency phonons which can be attributed to the low lying copper modes. The theoretical value of the slope dρ/dT deriving from the electron-phonon interaction is plotted by the solid curve. Although the data are widely dispersed, there is a clear trend in x: the slope is almost x independent for x>0.15, but increases as the insulator is approached. Our theoretical result for dρ/dT has very weak x dependence as a result of the vanishing electron-phonon scattering rate and diverging transport mass as x→0. This is consistent with the data in the metallic regime, but it is inconsistent near the insulator. It is clear, therefore, the electron-phonon interaction alone cannot explain the resistivity data for x<0.15. The failure to explain x dependent resistivity slope from the electron-phonon interaction alone at small x can be traced to the behavior of the lifetime, rather than the plasma frequency (as seen from Figs. 9 and 10). This implies other mechanisms such as magnetic or electron-electron scattering[28] may be more important near the insulating limit. The slope data can be reasonably well fit by adding a phenomenological contribution to the lifetime. This "fit" is shown by the dotted line.

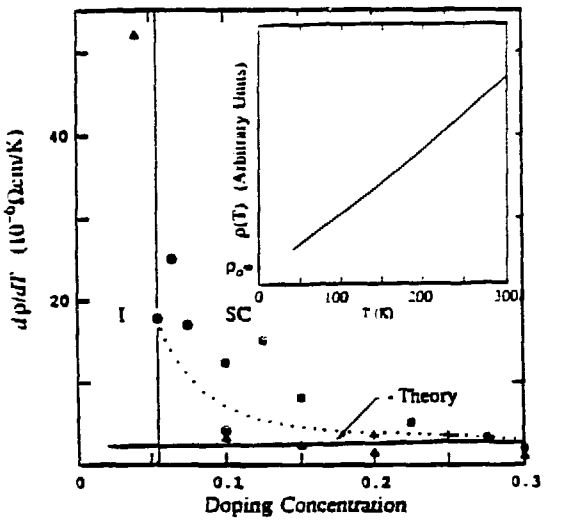

Fig. 11 Concentration dependence of the resistivity slope at 300K. Theoretical results with (or without) a small phenomenologically added lifetime plotted by the dotted line (or solid line). The data represented by triangles, circles, squares, and crosses are from Refs. 9, 27, 25, and 26, respectively. In the inset, the temperature dependent resistivity at x=0.2 calculated from the microscopically derived phonon spectral function is plotted.

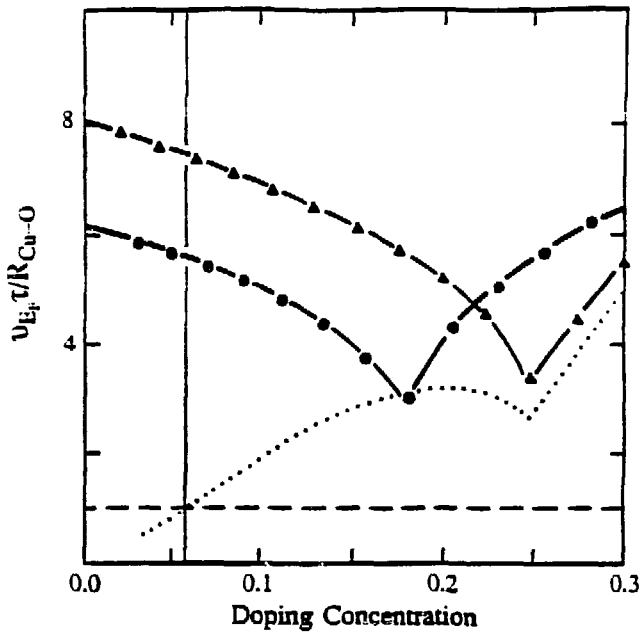

Fig. 12 Concentration dependence of the mean free path at 300K from electron-phonon interactions for t/V=0.25 (circles) and 0.50 (triangles). The dotted line is obtained from adding a small phenomenological lifetime to t/V=0.50 as in Fig. 11. The dashed line represents the Mott-Ioffe-Regel (MIR) condition. The dotted and MIR line intersect at the metal-insulator transition.

The mean free path, $l=v_F\tau$ for the quasiparticles is plotted in Fig. 12. Here we show the calculated result as a function of x at 300K for t/V=0.25 (circles) and 0.5 (triangles) in units of the copper-oxygen bond length, R_{Cu-O}. As noted before, the kinks in this figure reflect the van Hove singularities. We also plot the phenomenological result (dotted line) derived from adding $1/\tau_o$ to the electron-phonon background for t/V=0.50. The calculated mean free path l_{ph} from electron-phonon interactions shows that it is surprisingly close to the Mott-Ioffe-Regel (MIR) limit[29] which is shown by the dashed line. We find the mean free path ranges from 3 to 8 times the bond length. This small value of l_{ph} is consistent with the analysis of Gurvitch and Fiory in both La and Y based compounds. Since the MIR line separates metallic conductivity from insulating behavior, we may understand the metal-insulator transition by determining where the phenomenologically derived mean free path intercepts the dashed line. As shown in Fig. 12 this mean free path becomes shorter and shorter as the insulator is approached. It becomes comparable to the copper-oxygen bond length at x=0.05. This is the critical x where the system becomes insulating.

6. Summary and Conclusions

In this paper we have presented evidence in support of a generalized Fermi liquid picture for the copper oxides. Our proposed phase diagram suggests that unusual temperature and frequency dependent transport measurement do not imply the failure of a Fermi liquid picture for the would be-ground state (in the absence of superconductivity). Rather we view the normal state above T_c as having evolved gradually out of

the Fermi liquid phase as either temperature or doping concentration is varied.

The emphasis of this paper has been on the effects of very strong Coulomb correlations on electron-phonon interactions and the implications for transport properties. In our Fermi liquid approach, both a semi-realistic Coulomb renormalized band structure and a Brinkman-Rice or Mott localization transition at the half filled limit are included. Based on our self-consistent frozen phonon scheme, we argue that Coulomb correlations tend to suppress charge fluctuations within the copper-oxygen plane, thereby, reducing the electron-phonon coupling coupling constant as the metal-insulator is approached.

Our Mott localization picture is consistent with the concentration dependent plasma frequency $\omega_p^2 \propto x^{1/2}$ as found in both $La_{2-x}Sr_xCuO_4$ and $YBa_2Cu_3O_{7-\delta}$. Our calculations of the electron-phonon contribution to the resistivity $\rho \propto 1/\omega_p^2\tau$, show that electron-phonon coupling becomes weak as $x \rightarrow 0$. Therefore, these two competing effects in the lifetime and plasma frequency are partially canceled and the resistivity becomes almost concentration independent. Due to the presence of a high density of low frequency Copper-like modes, the electron-phonon component of the resistivity is quasi-linear down roughly to 50K.

While the electron-phonon contribution to the resistivity slope accounts for most of the observed value in the metallic regime ($x>0.15$), it is unable to explain the large value observed as the metal-insulator transition is approached ($x<0.15$). This suggests that other scattering mechanisms would be more important than phonons at small x. Based on our phenomenological fit to data we suggest an additional scattering rate of the form $1/\tau_o = N(E_F)T$.

Our mean free path calculations have led us to conclude that at low x, the metallic copper oxides are on the verge of satisfying the Mott-Ioffe-Regel condition. Our transport calculations combined with experimental data provide evidence that the metal-insulator transition coincides with the onset of this (MIR) condition for a hole concentration $x \sim 0.05$.

If our calculated transport electron-phonon coupling has a direct relation to the superconducting coupling constant λ_{sc} then the small value of the transport λ predicted from this work suggests that superconductivity from a phonon mediated mechanism, alone, would be difficult to understand.

7. Acknowledgements

We thank G. Thomas for providing us with his data. Useful conversations with T.F. Rosenbaum and S. Nagel are acknowledge. JHK wishes to thank the David and Lucile Packard Foundation for support.

8. References

1. R.J. Birgeneau and G. Shirane, *physical Properties of High Temperature Superconductors*, ed. D.M. Ginsberg (World Scientific, Singapore, 1989).

2 C.M. Varma, P.B. Littlewood, S. Schmitt-Rink, E. Abrahams and A.E. Rucken-

stein, *Phys. Rev. Lett.* 63 (1989) 1996.

3. Q. Si, J.H. Kim, J.P. Lu and K. Levin, *Phys. Rev.* **B42** (1990) 1033.
4. G.R. Stewart, *Rev. Mod. Phys.* 56 (1984) 755.
5. J.H. Kim, K. Levin, R. Wentzcovitch and A. Auerbach, *Phys. Rev.* **B40** (1989) 11378 ; J.H. Kim, K. Levin, R. Wentzcovitch and A. Auerbach (unpublished).
6. J.P. Lu, Q. Si, J.H. Kim and K. Levin, *Phys. Rev. Lett.* 65 (1990) 2466; J.P. Lu, Q. Si, J.H. Kim and K. Levin (unpublished)
7. see J.H. Kim, Ph.D. Thesis, University of Chicago (1990).
8. R.J. Cava, B. Battlogg, R.B. van Dover, D.W. Murphy, S. Sunshine, T. Siegrist, J.P. Remeika, E.A. Rietman, S. Zahurak and G.P. Espinosa, *Phys. Rev. Lett.* 58 (1987) 1676.
9. M. Suzuki, *Phys. Rev.* **B39** (1989) 2312.
10. Y. Kubo, Y. Shimakawa, T. Manakako, T. Satoh, S. Iijima, T. Ichiashi and H. Igarashi, *Physica* C164–166 (1989) 991.
11. M.C. Aronson, J.D. Thompson, J.L. Smith, and Z. Fisk *Phys. Rev. Lett.* 63 (1989) 2311.
12. A.B. Kaiser and S. Doniach, *Int. J. Magn.* 1 (1970) 11.
13. P.E. Sulewski, A.J. Sievers, M.B. Maple, M.S. Torikachvili, J.L. Smith and Z. Fisk, *Phys. Rev.* **B38** (1988) 5338.
14. A.M. Awasthi, W. P. Beyermann, J.P. Carini and G. Gruner, *Phys. Rev.* **B39** (1989) 2377.
15. M. Gurvitch and A.T. Fiory, *Phys. Rev. Lett.* 59 (1987) 1337 and see references therein.
16. G. Thomas (unpublished).
17. J.H. Kim, K. Levin and A. Auerbach, *Phys. Rev.* **B39** (1989) 11633.
18. W.F. Brinkman and T.M. Rice, *Phys. Rev.* **B2** (1970) 1324.
19. P. Coleman, *Phys. Rev.* **B29** (1984) 3035; S.E. Barnes, *J. Phys.* **F6** (1976) 1375; *ibid* 7 (1977) 2632.
20. R.E. Cohen, W.E. Pickett, H. Krakawer and L.L. Boyer, *Physica* **B150** (1988) 61.
21. J.C. Slater and G.F. Koster, *Phys. Rev.* 94 (1954) 1498.
22. B. Ranker, F. Gompf, E. Gering, N. Nucker, D. Ewert, W. Reichardt and H. Rietschel, *Z. Phys.* **B** (1987) 15.
23. J. Orenstein, G.A. Thomas, A.J. Millis, S.L. Cooper, D.H. Rapkine, T. Timusk, L.F. Schneemeyer, and J.V. Wasczak (unpublished).
24. M. Suzuki, *Strong Correlation and Superconductivity*, Edited by H. Fukuyama, S. Maekawa, and A.P. Malozemoff, (Springer-Verlag, New York, 1989).
25. J.M. Tarascon, L.H. Greene, W.R. McKinnon, G.W. Hull and T.H. Geballe, *Science* 235 (1987) 1373.
26. C. Uher, A.B. Kaiser, E. Gmelin and L. Walz, *Phys. Rev.* **B36** (1987) 5676.

27. B. Ellman, H.M. Jaeger, D.P. Katz, T.F. Rosenbaum, A.S. Copper and G.P. Espinosa, *Phys. Rev.* B39 (1989) 9012.

28. Q. Si and K. Levin (unpublished).

29. N.F. Mott and E.A. Davis, *Electronic Processes in Non-crystalline Materials* (Clarendon, Oxford, 1979); A.F. Ioffe, and A.R. Regel, *Prog. Semicond.* 4 (1960) 237.

DISCLAIMER